

**Coulomb excitation of  $^{44}\text{Ca}$  and  $^{46}\text{Ar}$** 

S. Calinescu,<sup>1,2</sup> L. Cáceres,<sup>3</sup> S. Grévy,<sup>4</sup> O. Sorlin,<sup>3</sup> Z. Dombrádi,<sup>5</sup> M. Stanoiu,<sup>1</sup> R. Astabatyán,<sup>6</sup> C. Borcea,<sup>1</sup> R. Borcea,<sup>1</sup> M. Bowry,<sup>7</sup> W. Catford,<sup>7</sup> E. Clément,<sup>3</sup> S. Franchoo,<sup>8</sup> R. Garcia,<sup>9</sup> R. Gillibert,<sup>10</sup> I. H. Guerin,<sup>4</sup> I. Kuti,<sup>5</sup> S. Lukyanov,<sup>6</sup> A. Lepailleur,<sup>3</sup> V. Maslov,<sup>6</sup> P. Morfouace,<sup>8</sup> J. Mrazek,<sup>11</sup> F. Negoita,<sup>1</sup> M. Niikura,<sup>8</sup> L. Perrot,<sup>8</sup> Z. Podolyák,<sup>7</sup> C. Petrone,<sup>1,2</sup> Y. Penionzhkevich,<sup>6</sup> T. Roger,<sup>3</sup> F. Rotaru,<sup>1</sup> D. Sohler,<sup>5</sup> I. Stefan,<sup>8</sup> J. C. Thomas,<sup>3</sup> Z. Vajta,<sup>5</sup> and E. Wilson<sup>7</sup>

<sup>1</sup>Horia Hulubei National Institute for Physics and Nuclear Engineering, P.O. Box MG-6, 077125 Bucharest-Magurele, Romania

<sup>2</sup>Faculty of Physics, University of Bucharest, Romania

<sup>3</sup>Grand Accélérateur National d'Ions Lourds (GANIL), CEA/DSM-CNRS/IN2P3, B.P. 55027, F-14076 Caen Cedex 5, France

<sup>4</sup>Centre d'Études Nucléaires de Bordeaux Gradignan-UMR 5797, CNRS/IN2P3, Université de Bordeaux 1, Chemin du Solarium, B.P. 120, 33175 Gradignan, France

<sup>5</sup>Institute for Nuclear Research, Hungarian Academy of Sciences, P.O. Box 51, Debrecen, H-4001, Hungary

<sup>6</sup>FLNR, JINR, 141980 Dubna, Moscow region, Russia

<sup>7</sup>Department of Physics, University of Surrey, Guildford GU2 7HX, United Kingdom

<sup>8</sup>Institut de Physique Nucléaire, CNRS/IN2P3, Université Paris-Sud, F-91406 Orsay, France

<sup>9</sup>KU Leuven, Instituut voor Kern-en Stralingsfysica, B-3001 Heverlee, Belgium

<sup>10</sup>Université de Caen Basse Normandie, Caen, France

<sup>11</sup>Nuclear Physics Institute, AS CR, CZ 25068, Rez, Czech Republic

(Received 29 September 2015; revised manuscript received 3 March 2016; published 25 April 2016)

The reduced transition probabilities  $B(E2; 0_{\text{g.s.}}^+ \rightarrow 2_1^+)$  of the  $^{46}\text{Ar}$  and  $^{44}\text{Ca}$  nuclei were studied using the Coulomb excitation technique at intermediate energy at the LISE/GANIL facility. The in-flight  $\gamma$  rays, emitted after the Coulomb excitation of their first  $2^+$  states, were detected in an array of 64  $\text{BaF}_2$  crystals. The present  $B(E2 \uparrow)$  value for  $^{44}\text{Ca}$ ,  $475(36) \text{ e}^2\text{fm}^4$ , agrees well with the value of  $495(35) \text{ e}^2\text{fm}^4$  obtained by averaging results of previous experiments. Consistent  $B(E2; 0_{\text{g.s.}}^+ \rightarrow 2_1^+)$  values of  $225(29) \text{ e}^2\text{fm}^4$  and  $234(19) \text{ e}^2\text{fm}^4$  have been obtained for  $^{46}\text{Ar}$  from an absolute and a relative measurement, normalized to the  $^{44}\text{Ca}$  value. Both results agree with the ones obtained with the same experimental technique at the NSCL facility but are a factor of 2 smaller than the shell model predictions. The drop in  $B(E2; 0_{\text{g.s.}}^+ \rightarrow 2_1^+)$  in the Ar chain at  $N = 28$ , confirmed in this experiment, shows that  $^{46}\text{Ar}$  is sensitive to the  $N = 28$  shell closure.

DOI: [10.1103/PhysRevC.93.044333](https://doi.org/10.1103/PhysRevC.93.044333)

**I. INTRODUCTION**

The evolution of the  $N = 28$  shell closure has been investigated far from stability using several experimental techniques. Experimental results suggest that a progressive onset of deformation occurs below  $^{48}\text{Ca}$  (see, e.g., Ref. [1]). In particular, the gradual decrease of the  $2_1^+$  energies in the  $N = 28$  isotones from 3831 keV in  $^{48}\text{Ca}$ , 1577 keV in  $^{46}\text{Ar}$  [2], 1329 keV in  $^{44}\text{S}$  [3], and 770 keV in  $^{42}\text{Si}$  [4,5] indicates that a large deformation is steadily establishing toward  $^{42}\text{Si}$ .

Mean field approaches [6–9] as well as shell model calculations [10–14] predict a close-to-spherical  $^{46}\text{Ar}$ , a shape mixing or shape coexistence in  $^{44}\text{S}$ , and a large oblate deformation in  $^{42}\text{Si}$ . The properties of the recently discovered low-lying isomeric  $0_2^+$  state in  $^{44}\text{S}$  [15] supports a shape mixing between the  $0_1^+$  and  $0_2^+$  states.

Being located two protons away from the doubly magic  $^{48}\text{Ca}$ ,  $^{46}\text{Ar}$  should in principle be considered as a semimagic nucleus, as confirmed by the following experimental results. A significant drop in the one-neutron separation energy  $S_n$  is observed in the Ar chain after having passed  $N = 28$  [16], which is suggestive of a shell closure. Moreover, studies of its neutron Fermi surfaces via various transfer and knockout reactions [17–19] on  $^{46}\text{Ar}$  led to the following conclusions: (i) the neutron  $f_{7/2}$  orbit is about 75% full in the ground state of  $^{46}\text{Ar}$ , the remaining 25% being in the  $p_{3/2}$  orbit, (ii) the

$N = 28$  gap between the  $f_{7/2}$  and  $p_{3/2}$  orbits only decreases by about 330 keV between  $^{46}\text{Ar}$  and  $^{48}\text{Ca}$ , therefore remaining larger than 4 MeV. The systematics of  $2_1^+$  energies and  $B(E2; 0_{\text{g.s.}}^+ \rightarrow 2_1^+)$  values give further support to the existence of a shell closure at  $N = 28$  in the Ar isotopic chain. Indeed, an increase in  $2^+$  excitation energy is observed for  $^{46}\text{Ar}$ , while a drop in  $B(E2; 0_{\text{g.s.}}^+ \rightarrow 2_1^+)$  is derived using the values of  $196(39) \text{ e}^2\text{fm}^4$  [2] and  $218(31) \text{ e}^2\text{fm}^4$  [20], obtained from intermediate energy Coulomb excitation measurements. As for the protons, it was discussed in Refs. [17,21] that the  $d_{3/2}$  and  $s_{1/2}$  orbits are likely degenerate and equiprobably occupied.

Two things are, however, shedding doubts concerning our full understanding of the shell structure of  $^{46}\text{Ar}$ . On the experimental side, a high  $B(E2; 0_{\text{g.s.}}^+ \rightarrow 2_1^+)$  value of  $570_{-160}^{+335} \text{ e}^2\text{fm}^4$  [22] has been deduced from the lifetime of the  $2_1^+$  state obtained from the differential recoil-distance Doppler-shift method. This value differs by more than  $2\sigma$  from the two other experimental values. It is, however, in close agreement with the value of about  $500 \text{ e}^2\text{fm}^4$  predicted by shell-model calculations, in which no drop in  $B(E2; 0_{\text{g.s.}}^+ \rightarrow 2_1^+)$  at  $N = 28$  is predicted, regardless of the interaction used [10,12,13,23,24]. Given the presently uncertain situation, we remeasured the  $B(E2; 0_{\text{g.s.}}^+ \rightarrow 2_1^+)$  value of  $^{46}\text{Ar}$  in an absolute manner and relatively to the well-known value in  $^{44}\text{Ca}$ . The latter study is interesting as it suppresses most of the systematic

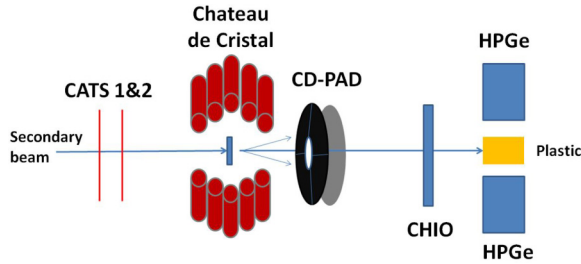


FIG. 1. Schematic picture of the experimental setup.

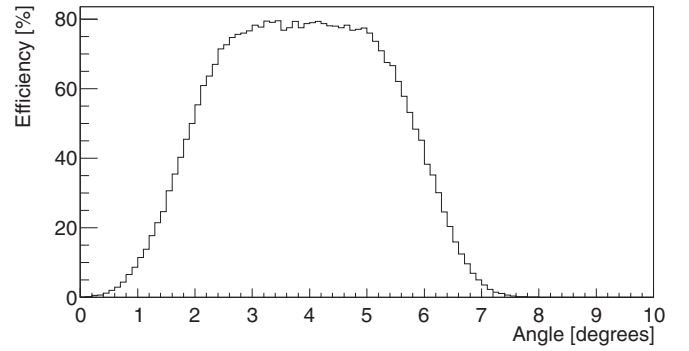
uncertainties inherent to the intermediate energy Coulomb excitation measurements.

## II. EXPERIMENT

The  $^{46}\text{Ar}$  nuclei were produced at the GANIL facility in the interactions of a 60 AMeV  $^{48}\text{Ca}^{19+}$  beam, at an average intensity of  $\sim 4 \mu\text{A}$ , in a 145- $\mu\text{m}$   $^9\text{Be}$  target. An additional setting of the spectrometer was required to select the stable  $^{44}\text{Ca}$  nucleus that was used for calibration purpose. Both  $^{46}\text{Ar}$  and nuclei  $^{44}\text{Ca}$  had similar midtarget energies of 38.5 MeV/A and 36.8 MeV/A, respectively. These nuclei were separated from other reaction products by the LISE3 spectrometer [25], in which a wedge-shaped Be degrader of 221  $\mu\text{m}$  was inserted at the intermediate focal plane. Their Coulomb excitation was induced by a 200-mg/cm $^2$   $^{208}\text{Pb}$  target placed at the image focal plane of the spectrometer that was surrounded by the 64 hexagonal  $\text{BaF}_2$  crystals of the Chateau de Cristal placed at a mean distance of 25 cm. In total,  $2.93 \times 10^8$   $^{46}\text{Ar}$  and  $2.5 \times 10^8$   $^{44}\text{Ca}$  were produced with purities of 83 and 64%, respectively.

A schematic picture of the experimental setup is shown in Fig. 1. Two position-sensitive CATS [26] detectors were placed 90 and 50 cm upstream of the Pb target to (i) determine the location of the ion impacts on target from their tracking, (ii) identify the nuclei from their time-of-flight (TOF) measurement with respect to the cyclotron radio-frequency, (iii) establish a time coincidence between the incoming nuclei and their in-flight emitted  $\gamma$ -rays, and (iv) count the number incident nuclei to determine reaction cross sections.

Scattered nuclei that encountered a Coulomb interaction in the Pb target were detected in a 500- $\mu\text{m}$ -thick annular double-sided silicon strip detector (DSSSD) [27], which had a central hole of 3-cm diameter. It consisted, on the front side, of 4 quadrants of 16 annular strips of 2 mm pitch each, on the rear side, of 24 radial strips of 3.4° pitch, each grouped three by three. The interstrip distance was 100  $\mu\text{m}$ . The detector was mounted at a distance of 41.2 cm from the secondary target. In this way the DSSSD covered angles from 1.5 to 6.5° in the laboratory frame. This angular coverage ensures that nuclei are detected up to the grazing angle of the reaction. The scattered ions were identified in an event-by-event basis by the combined measurements of their energy loss in the DSSSD ( $\Delta E$ ) and time of flight. The angular resolution of DSSSD ranged from 0.14 degrees for the most inner ring to 0.5 degrees for outer one. The DSSSD was followed by a detector that consisted of four nonsegmented silicon quadrants of 1500  $\mu\text{m}$  thick.

FIG. 2. Simulated efficiency of the DSSSD detector for  $^{44}\text{Ca}$  ions. Angles are given in the laboratory frame.

This aimed at detecting the residual energy of the scattered nuclei and determining their mass. Unfortunately, the signals from this detector were not exploitable for the analysis and a mass identification could not be made. Nuclei that passed through the central hole of the DSSSD were identified from their energy loss measured in a digitally processed ionization chamber (CHIO), and from their time of flight derived from the signals of a plastic scintillator located behind. A set of Ge detectors was placed around the plastic scintillator to confirm the identification procedure from the detection of known  $\gamma$ -rays emitted in the isomer de-excitation of the neighboring nucleus  $^{43}\text{S}$ .

A GEANT4 simulation was used to determine the geometrical efficiency of the DSSSD detector, considering its dead zones and the beam profile reconstructed at the target position. The detector response, first considered here in the case of an isotropic emission of ions, is presented in Fig. 2 as a function of the deflection angle of the  $^{44}\text{Ca}$  nuclei. It increases steeply between 0° and 2° and reaches a plateau at almost 80% between 3° and 5° in the laboratory frame.

When Coulomb excited, the first excited states of the  $^{46}\text{Ar}$  and  $^{44}\text{Ca}$  nuclei decayed in-flight by the emission of  $\gamma$  rays, which were detected by the 64  $\text{BaF}_2$  crystals of the Chateau de Cristal placed in two hemispheres around the target. With a time resolution of 1 ns, and a minimum target to detector distance of 25 cm, a time-of-flight separation between the prompt  $\gamma$ -rays and neutrons, possibly evaporated by the target, can be achieved [29].  $\gamma$ -ray energies detected promptly in two adjacent crystals were considered to be produced by a single  $\gamma$ -ray that encountered a Compton scattering. Their energies were then summed (add-back procedure), leading to a reduction of the Compton edge in the  $\gamma$ -ray spectra. The in-flight efficiency of the array was determined using a GEANT4 simulation, whose validity was checked first from the comparison between the simulated and measured efficiencies obtained from stationary calibration sources. The DWEIKO code [30] was used to determine the angular distribution of the emitted  $\gamma$ -rays, which was used subsequently as an input for the GEANT4 simulation. It was checked that the observed angular distribution match the calculated one. A photopeak efficiency of  $\sim 18\%$  is found at 1.157 MeV. According to the Doppler effect,  $\gamma$  peaks corresponding to the in-flight de-excitation of the  $2_1^+$  state at  $E_{\gamma_0} = 1157$  keV in  $^{44}\text{Ca}$

are shifted as a function of their detection angle. To achieve an optimized Doppler-shift correction, effective angles, at which  $\gamma$ -rays are detected in individual crystals, were determined using the detected peak energies  $E_\gamma$ :

$$\frac{E_\gamma}{E_{\gamma_0}} = \frac{\sqrt{1 - \beta^2}}{1 - \beta \cos \theta_\gamma}, \quad (1)$$

where  $\beta = v/c$  is the velocity of the nucleus relative to the speed of light. These angles were subsequently used to sum up the Doppler-corrected  $\gamma$  spectra corresponding to each detector. In this procedure, it was assumed that the  $\gamma$ -decay occurred at the target position, which is a reasonable approximation for a short-lived excited state. Effective angles can deviate from the purely geometrical ones owing to several effects, among which the mean detection depth of the  $\gamma$ -rays that depends on their energy.

When dealing with beams of intermediate energies, both Coulomb and nuclear interactions likely take place. The Coulomb interaction dominates over the nuclear interactions when the impact parameter  $b$  of the reaction is larger than the range of the nuclear force. Below this impact parameter, nuclear interactions could no longer be neglected, and the way it has been handled in our work will be described below. Using the prescriptions derived from Refs. [31,32], a minimal impact parameter  $b_{\min}$ , which depends on the interaction radius of the target and projectile, is obtained as follows:

$$b_{\min} = R_p + R_t + 6 + \frac{\pi a}{2\gamma} \text{ fm}, \quad (2)$$

with

$$R_{p(t)} = 1.28 A_{p(t)}^{1/3} - 0.76 + 0.8 A_{p(t)}^{-1/3} \text{ fm}, \quad (3)$$

where  $A_{p(t)}$  is the mass of the projectile and target, respectively, and

$$a = \frac{Z_p Z_t e^2}{\mu c^2 \beta^2}; \quad \gamma = \frac{1}{\sqrt{1 - \beta^2}}. \quad (4)$$

Here  $e$  is the electron charge,  $c$  the speed of light,  $\mu$  the reduced mass of the system, while  $Z_p$  and  $Z_t$  are the atomic mass number of the projectile and target.

Using semiclassical trajectories, the minimal impact parameter  $b_{\min}$ , below which the nuclear interaction adds to

Coulomb excitation [33], is linked to a maximal scattering angle  $\theta_{\text{lab}}^{\max}$ , beyond which nuclear excitations dominate. At small scattering angles, as those discussed in the present work, the approximation proposed in Ref. [34] holds:

$$\theta_{\text{lab}}^{\max} = \frac{2Z_p Z_t e^2}{b_{\min} \mu c^2 \beta^2 \gamma}. \quad (5)$$

### III. RESULTS

#### A. Coulomb excitation of $^{44}\text{Ca}$

The left part of Fig. 3 displays the Doppler-corrected and background-subtracted  $\gamma$  spectra of  $^{44}\text{Ca}$  as a function of the scattering angle, casted in intervals of  $1^\circ$ . A weak  $\gamma$ -ray background component, obtained by gating on an off-prompt time window, was subtracted in these spectra. Above  $1^\circ$ , the peak corresponding to the  $2^+$  energy becomes clearly visible and remains present afterwards. Using the present mean velocity value  $\langle \beta \rangle$  of 0.273 in Eqs. (2) and (5), it is found that the Coulomb process dominates for impact parameters larger than  $b_{\min} = 18.4$  fm, i.e., for maximum deflection angle  $\theta_{\text{lab}}^{\max} = 4.0^\circ$ . Note that this value is significantly smaller than the grazing angle of the reaction that is  $6.1^\circ$ . The Doppler-corrected  $\gamma$  spectrum presented in the right part of Fig. 3 is obtained when restricting to events with deflection angles up to  $\theta_{\text{lab}}^{\max} = 4.0^\circ$ .

The  $B(E2; 0_{\text{g.s.}}^+ \rightarrow 2_1^+)$  value of  $^{44}\text{Ca}$  is obtained from the comparison between experimental and theoretical differential cross sections. The latter were calculated with the DWEIKO code that use the optical potential parameters optimized for the  $^{40}\text{Ar} + ^{208}\text{Pb}$  [35] system as input. The same Coulomb and nuclear potential parameters were used: a surface diffuseness of  $a = 0.55$  fm, a radius parameter of  $r_0 = 1.2$  fm, and real and imaginary potential depths of  $V_0 = 74.3$  MeV and  $W_0 = 69.3$  MeV, respectively. To allow the comparison between theoretical and experimental cross sections (see Fig. 4), theoretical cross sections were implemented in a GEANT4 [28] simulation that take into account effects caused by the incoming beam angle, its spatial extension, its angular straggling in the target, the geometry of the DSSSD, as well as the  $\gamma$ -ray detector efficiency. In a first step only the Coulomb contribution was considered in the theory. The best agreement

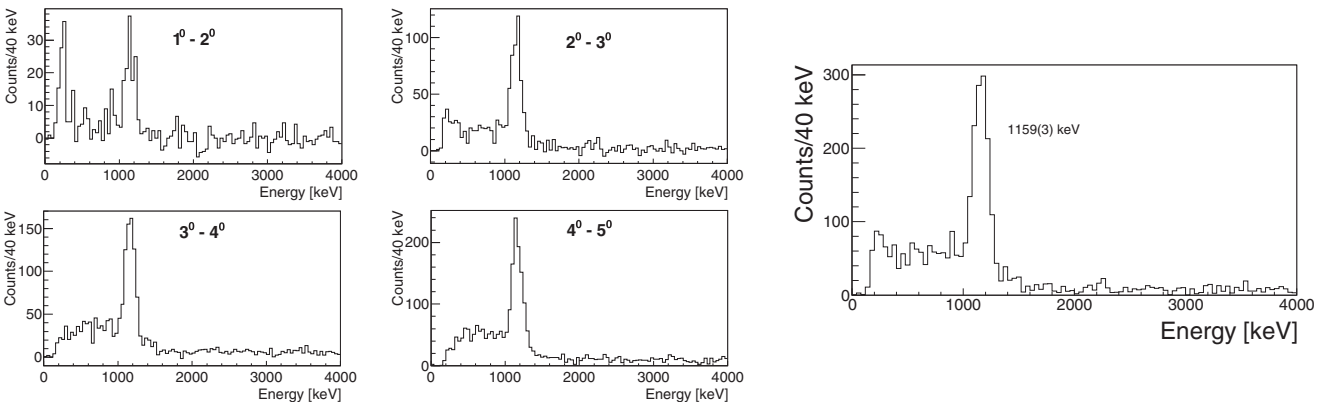


FIG. 3. Left: The Doppler corrected and background subtracted  $\gamma$ -ray spectra are displayed as a function of the  $^{44}\text{Ca}$  scattering angles, in ranges of  $1^\circ$ . Right: Same for scattering angles between  $\theta_{\text{lab}} = 1.0^\circ$  and  $\theta_{\text{lab}}^{\max} = 4.0^\circ$ .

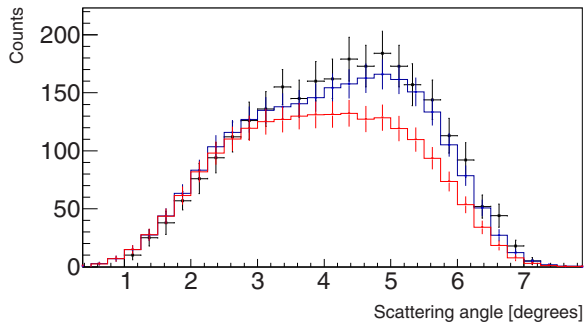


FIG. 4. Comparison between the calculated angular distribution in laboratory frame (red line) to experimental angular distribution (black crosses), obtained with a  $B(E2; 0_{g.s.}^+ \rightarrow 2_1^+)$  value of  $475 \text{ e}^2\text{fm}^4$  and neglecting nuclear excitations. To describe the experimental angular distribution over the whole angular range, a value of  $\beta_N = 0.35(4)$  was implemented for the nuclear contribution (blue line), keeping the Coulomb contribution constant.

between the calculated (red line of Fig. 4) and the experimental (black crosses) cross sections of  $53(4) \text{ mb}$  is found in the  $1^\circ$ – $3^\circ$  region using a  $B(E2; 0_{g.s.}^+ \rightarrow 2_1^+)$  value of  $475(36) \text{ e}^2\text{fm}^4$ . This result is in excellent agreement with the value of  $473(20) \text{ e}^2\text{fm}^4$  [ $\beta_C = 0.253(5)$ ] adopted in the compilation of Raman *et al.* [36], as well as with the values obtained via Coulomb excitation [37,38], Doppler-shift attenuation method [39–41], electron [42,43], and alpha scattering [44].

Beyond  $3^\circ$ , experimental and theoretical cross sections progressively deviate, owing to the fact that the  $2^+$  state becomes excited by a combination of Coulomb and nuclear processes. An adjustable nuclear contribution  $\beta_N$  has, therefore, been added to the GEANT4 simulation until matching experimental cross section over the whole observed angular range. This leads to the blue line of Fig. 4, which is obtained with a nuclear excitation strength of  $\beta_N = 0.35(4)$ . This nuclear contribution,  $\beta_N$ , is larger than that of Coulomb one,  $\beta_C = 0.253(5)$  [36], thus indicating that the  $0_1^+ \rightarrow 2_1^+$  excitation is dominantly excited via neutron excitations. This is in line with what is expected for a  $Z = 20$  proton closed-shell nucleus. We note here that the deviation to pure Coulomb contribution, which already occurs slightly below  $\theta_{\text{lab}}^{\text{max}}$ , is also partly due to

the angular straggling encountered by the ions traversing the reaction target.

We examine here the possible contamination of the peak corresponding to the  $2_1^+$  state at  $1157 \text{ keV}$  in  $^{44}\text{Ca}$  from the feeding of states coming from above, and decaying through it. If populated, the  $2_2^+$  state at  $2656.5 \text{ keV}$  decays by 90% to the  $2_1^+$  state via a  $1499.5\text{-keV}$   $\gamma$ -ray transition [45]. At intermediate energies, the one-step Coulomb excitation dominates. As a result, the population of the  $2_2^+$  states at  $2656.5 \text{ keV}$  will occur directly from the ground state, if the  $B(E2; 0_{g.s.}^+ \rightarrow 2_2^+)$  value is large enough. We do not see evidence of such a  $1499.5\text{-keV}$   $\gamma$ -ray in Fig. 3. Using a GEANT4 simulation, we establish our sensitivity limit to 95 counts in the  $\gamma$  spectrum, meaning that a peak would have been observed if above 95 counts. This nonobservation corresponds to an upper  $B(E2; 0_{g.s.}^+ \rightarrow 2_2^+)$  value of about  $41 \text{ e}^2\text{fm}^4$ , which is consistent with the value of  $41(9) \text{ e}^2\text{fm}^4$  reported in Ref. [46]. In principle, we should then subtract this contribution to the present  $B(E2; 0_{g.s.}^+ \rightarrow 2_1^+)$ , thus reducing the  $B(E2; 0_{g.s.}^+ \rightarrow 2_1^+)$  value by a bit less than 10%. However, as we and none of the authors of Refs. [36–44] could confirm this feeding of this  $2_2^+$  from the ground state, this contribution has not been subtracted.

## B. Coulomb excitation of $^{46}\text{Ar}$

The study of the Coulomb excitation of the  $^{46}\text{Ar}$  nucleus was achieved by using the same procedure as for  $^{44}\text{Ca}$ . With a mean  $\beta = v/c$  value of  $0.279$ , a minimum impact parameter  $b_{\text{min}} = 18.17 \text{ fm}$ , and a maximum scattering angle  $\theta_{\text{lab}}^{\text{max}} = 3.25^\circ$  are found from Eqs. (2) and (5). The Doppler-corrected background-subtracted  $\gamma$  spectra are shown for different angular ranges in the left part of Fig. 5. Along with the  $1577 \text{ keV}$  peak associated with the de-excitation of the  $2^+$  state to the ground state in  $^{46}\text{Ar}$ , a peak is seen at  $542 \text{ keV}$ , the amplitude of which grows with increasing angles. This transition corresponds to the de-excitation of the first excited state in the  $^{45}\text{Ar}$  nucleus, observed in the in-flight  $\gamma$ -ray spectroscopy of  $^{45}\text{Ar}$  [47], in the one-neutron removal reaction from  $^{46}\text{Ar}$  [19], as well as in the  $^{44}\text{Ar}$  stripping reaction [48]. As can be seen in the right part of Fig. 5, this transition is

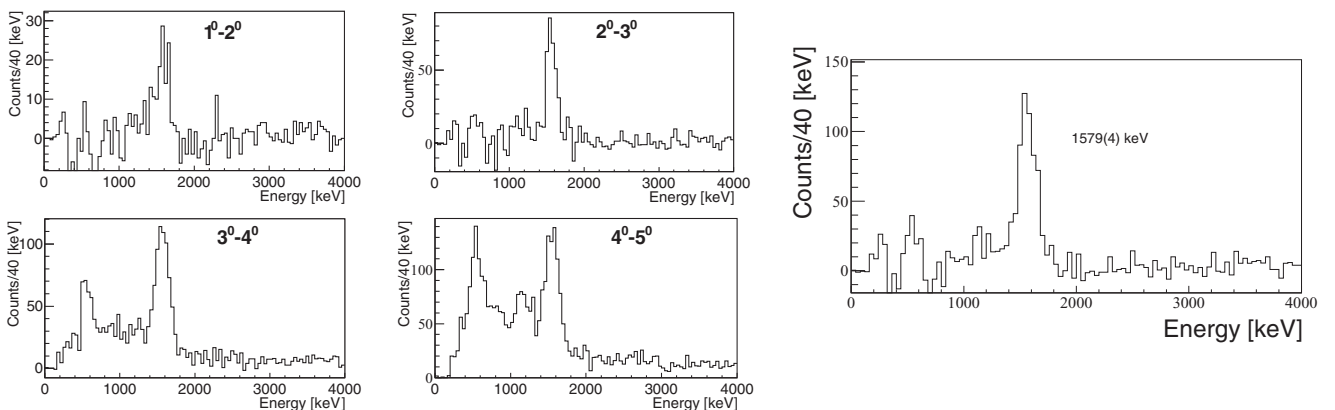


FIG. 5. Left: Doppler-corrected background subtracted  $\gamma$ -ray spectra displayed as a function of the scattering angle of  $^{46}\text{Ar}$ , cast in fixed angular ranges of  $1^\circ$ . Right: Same between scattering angles of  $\theta_{\text{lab}} = 1^\circ$  and  $\theta_{\text{lab}} = 3.25^\circ$ .

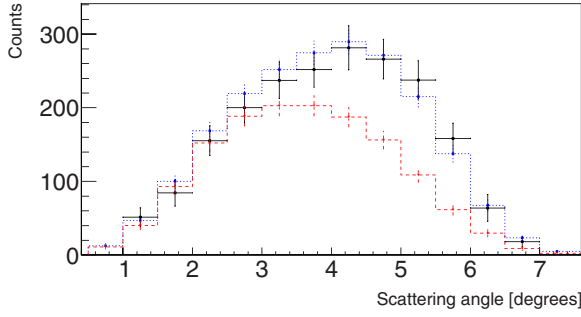


FIG. 6. Comparison between the calculated angular distribution in laboratory frame (red line) to the experimental angular distribution (black crosses) obtained by using a  $B(E2; 0_{g.s.}^+ \rightarrow 2_1^+)$  value of  $225 \text{ e}^2\text{fm}^4$  and by neglecting nuclear excitations. To describe the experimental angular distribution over the whole angular range, a value of  $\beta_N = 0.25(6)$  was implemented for the nuclear contribution (blue line), keeping the Coulomb contribution unchanged.

not present in the energy spectrum for  $\theta_{\text{lab}} < 3^\circ$ , suggesting that the  $^{45}\text{Ar}$  nucleus is populated by a nuclear reaction, such as the removal of one neutron from  $^{46}\text{Ar}$ . The peak, possibly observed around 1200 keV, may be due to the feeding of the 1770.3 keV state as well, that decays in 100 % cases to the 542-keV state.

As seen in Fig 6, the nuclear contribution could no longer be neglected even below  $\theta_{\text{lab}}^{\text{max}} = 3.25^\circ$ , as the angular straggling is bringing some of the nuclear contribution below this angle. Therefore, the Coulomb contribution is extracted from a fit between calculated and experimental cross sections over a slightly smaller angular range, from  $1^\circ$  up to  $\theta_{\text{lab}} = 3^\circ$ . A  $B(E2; 0_{g.s.}^+ \rightarrow 2_1^+)$  value of  $225(29) \text{ e}^2\text{fm}^4$  is derived from the integrated cross section of  $40(5) \text{ mb}$ . A compatible  $B(E2; 0_{g.s.}^+ \rightarrow 2_1^+)$  value of  $234(19) \text{ e}^2\text{fm}^4$  [or  $\beta_C = 0.189(15)$ ] is derived for  $^{46}\text{Ar}$ , in relative to the one of  $473(20) \text{ e}^2\text{fm}^4$  [36] for  $^{44}\text{Ca}$ , after having considered the minor differences in efficiencies involved in the two cases. The  $B(E2; 0_{g.s.}^+ \rightarrow 2_1^+)$  values obtained via the two methods overlap within one  $\sigma$  uncertainty. Both results are furthermore compatible with the values of  $196(39) \text{ e}^2\text{fm}^4$  [2] and  $218(31) \text{ e}^2\text{fm}^4$  [20] obtained at intermediate energy Coulomb excitation. Averaging of our two  $B(E2)$  values with the two previous ones leads to  $B(E2)$  value of  $216(22) \text{ e}^2\text{fm}^4$ , which is about half of the one deduced from lifetime measurement,  $B(E2) = 570_{-160}^{+335} \text{ e}^2\text{fm}^4$  [22]. Since the latter value has a very large error bar, results remain almost compatible within  $2\sigma$ . The measured reduced transition probabilities  $B(E2; 0_{g.s.}^+ \rightarrow 2_1^+)$  in  $^{46}\text{Ar}$ , obtained in all the discussed experimental works (including ours), are presented in Table I. As in the case of  $^{44}\text{Ca}$ , we clearly see from Fig. 6 that a nuclear contribution has to be considered above  $3^\circ$ . In order to reproduce the experimental cross sections over the full angular range, a nuclear contribution of  $\beta_N = 0.25(6)$  must be introduced. As for the case of  $^{44}\text{Ca}$ , the nuclear contribution is larger than the Coulomb one.

We examine here the possibility of a side-feeding of the  $2_1^+$  state at 1577 keV in  $^{46}\text{Ar}$  from a tentatively assigned  $2_2^+$  state at 3489 keV [47]. If populated directly from the ground state, this state at 3489 keV would decay, according to Ref. [47],

TABLE I. Measured  $B(E2; 0_{g.s.}^+ \rightarrow 2_1^+)$  values, in units of  $\text{e}^2\text{fm}^4$ , obtained for  $^{46}\text{Ar}$  from different experiments and the from present work, in relative to  $^{44}\text{Ca}$  (Rel.) or in absolute (Abs.). The  $\langle B(E2) \rangle$  value is obtained by averaging the present absolute and relative  $B(E2)$  values with the  $B(E2)$  values derived in Refs. [2,20]

Ref.	[2]	[20]	[22]	[Rel.]	[Abs.]	$\langle B(E2) \rangle$
$B(E2)$	196(39)	218(31)	$570_{-160}^{+335}$	234(19)	225(29)	216(22)

through a 1912-keV transition by 40%. Such a  $\gamma$ -ray is not observed in our spectrum of Fig. 5. Based on a GEANT 4 simulation, our limit of nonobservation of such a peak is 52 counts. It corresponds to a maximum  $B(E2; 0_{g.s.}^+ \rightarrow 2_2^+)$  value of  $23 \text{ e}^2\text{fm}^4$ , which would reduce the  $B(E2; 0_{g.s.}^+ \rightarrow 2_1^+)$  value of  $^{46}\text{Ar}$  by 10% at most.

#### IV. DISCUSSION

Experimental  $2_1^+$  energies of the Ar isotopes were compared to nuclear shell model calculations using the effective interactions SDPFU [10], SDPFMU [13], and SDPFK [12] that were developed to describe nuclei in the  $sd$ - $pf$  valence space. These calculations have been carried out with the shell model code NuShellX [49], using neutron and proton polarization charges  $\delta_n = \delta_p = 0.5e$  that are the default values for this region [12]. The calculated  $E(2_1^+)$  values differ by up to 30% along the isotopic chain, depending on the choice of interaction [53]. Nevertheless, the global evolution of the  $E(2_1^+)$  energy as a function of the neutron number  $N$  is rather well reproduced.

As shown in Fig. 7, calculated  $B(E2; 0_{g.s.}^+ \rightarrow 2_1^+)$  values display, despite large fluctuations that depend on the choice of interaction, very similar trends. Surprisingly, all interactions predict a similar  $B(E2)$  value at  $N = 28$  that is the largest in

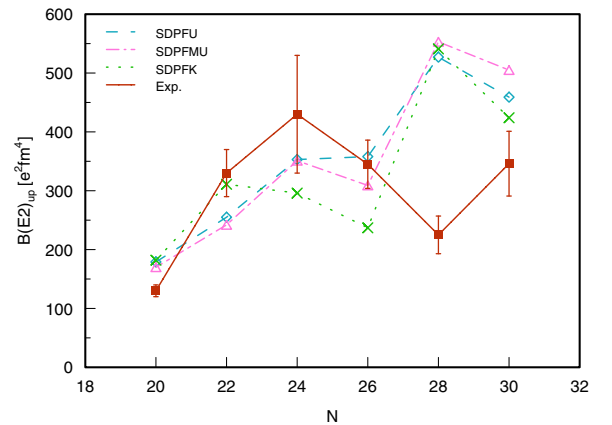


FIG. 7. Measured and calculated  $B(E2; 0_{g.s.}^+ \rightarrow 2_1^+)$  values for the Ar isotopes using SDPFK, SDPFMU, and SDPFU interactions with standard polarization charges  $\delta_n = \delta_p = 0.5e$ . The  $B(E2; 0_{g.s.}^+ \rightarrow 2_1^+)$  values are taken from Ref. [36] for  $^{36} - ^{44}\text{Ar}$  and from Ref. [53] for  $^{48}\text{Ar}$ . The experimental value presented for  $^{46}\text{Ar}$  corresponds to the weighted average value from Refs. [2,20] and from the present work.

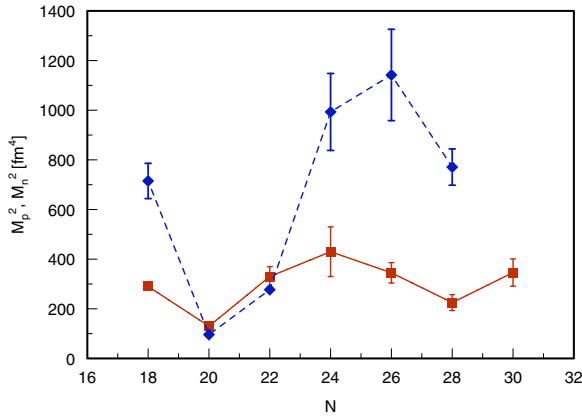


FIG. 8. Square of the phenomenological proton (continuous red line) and neutron (dotted blue line) transition matrix elements. The  $M_p^2$  values are for  $^{36-44}\text{Ar}$  [36], for  $^{46}\text{Ar}$  extracted from the average  $B(E2; 0_{\text{g.s.}}^+ \rightarrow 2_1^+)$  value obtained from the Coulomb excitation experiments, and for  $^{48}\text{Ar}$  [53].

the Ar chain, but this is precisely where the deviation to the experimental  $B(E2)$  is the largest.

To get some insight into the reason of this deviation, the structure of the  $0_{\text{g.s.}}^+ \rightarrow 2_1^+$  transition has been decomposed into the corresponding proton and neutron interaction strengths. The  $B(E2)$  value is linked to the proton transition matrix element  $M_p$ ,  $B(E2) = e^2 M_p^2$ , while the combination of inelastic ( $p, p'$ ) and Coulomb excitation studies allow to determine the ratio of neutron to proton matrix elements  $M_n/M_p$ . This ratio has been derived for the  $^{36,40,42,44}\text{Ar}$  nuclei by Khan *et al.* [50] and for the  $^{46}\text{Ar}$  nucleus by Riley *et al.* [51]. Adding the information on the  $B(E2)$  values, the neutron transition matrix elements  $M_n$  have been deduced. As for  $^{38}\text{Ar}$ , the mirror nucleus relation [52] was used to deduce its  $M_n$  value. The evolution of phenomenological proton  $M_p^2$  and neutron  $M_n^2$  transition probabilities is shown in Fig. 8. Kinks in the proton and neutron transition matrix elements are observed at the  $N = 20$  and  $N = 28$  neutron closed shells. The amplitude of the  $M_p^2$  depletions at the neutron closed shells are smaller than those of the  $M_n^2$  values, owing to the fact that protons are only indirectly sensitive to the closed shell, in contrary to neutrons.

In the generalized effective charge model [54] both the proton and neutron quadrupole matrix elements are interrelated due to the polarization carried by each nucleon. In this model,

$$M_p = (1 + \delta_p)A_p + \delta_n A_n; \quad M_n = \delta_p A_p + (1 + \delta_n)A_n, \quad (6)$$

where  $\delta_p$  and  $\delta_n$  are the proton and neutron polarization charges, and  $A_p$  and  $A_n$  are the quadrupole transition matrix elements for protons and neutrons, respectively. Using Eq. (6) and appropriate polarization charges, the  $A_n, A_p$  matrix elements can be determined, thus allowing the respective roles of the protons and neutrons to be extracted. The square of these matrix elements, obtained with standard  $\delta_n = \delta_p = 0.5$  polarization charges, is compared to those calculated within the shell model using the SDFPU interaction in Fig. 9. Matrix element obtained using effective charges of  $\delta_n = 0.8$  and

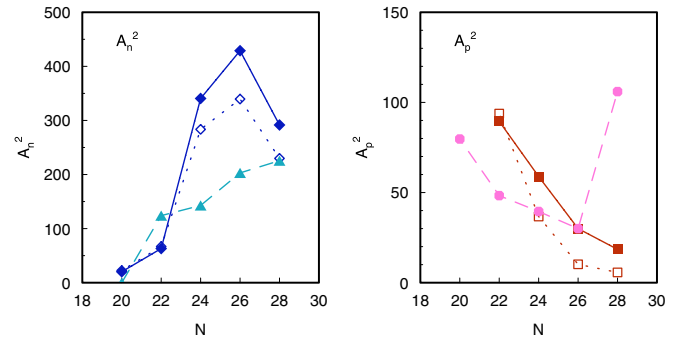


FIG. 9. Comparison of the square of the quadrupole matrix elements (given in  $\text{e}^2\text{fm}^4$ ) deduced for protons and neutrons using the standard  $\delta_n = \delta_p = 0.5$  polarization charges (solid line) and the  $\delta_n = 0.8, \delta_p = 0.2$  polarization charges proposed by Riley *et al.* [51] (dotted line) with those calculated within the shell model using the SDFPU interaction (dashed line).

$\delta_p = 0.2$  as in Ref. [51], are shown as well in Fig. 9. It is found that, independently of the used  $\delta_{n,p}$  values, the  $A_n$  values are steeply rising from  $N = 20$  to  $26$  and decrease at  $N = 28$ . In the shell model calculation,  $A_n$  increases steadily from  $N = 20$  to  $N = 28$ , where it agrees with the experimental value. Proton matrix elements  $A_p^2$  are globally weaker than  $A_n^2$ . As shown on the righthand side of Fig. 8, experimental values decrease steadily from  $N = 20$  to  $28$ . This trend is in agreement with the shell model calculations up to  $N = 26$ , where a sudden increase in  $A_p^2$  is calculated instead. The main reason for the too large calculated  $B(E2)$  value at  $N = 28$  should be found in this large deviation of  $A_p^2$  at  $N = 28$ .

## V. CONCLUSIONS

In summary, a reduced transition probability  $B(E2; 0_{\text{g.s.}}^+ \rightarrow 2_1^+)$  of  $475(36) \text{e}^2\text{fm}^4$  has been determined for  $^{44}\text{Ca}$  by using the intermediate energy Coulomb excitation technique at GANIL. It matches very well the adopted value of  $473(20)\text{e}^2\text{fm}^4$  [36] and the weighted average value obtained from all experiments,  $495(35)\text{e}^2\text{fm}^4$ . Consistent  $B(E2)$  values of  $225(29) \text{e}^2\text{fm}^4$  and  $234(19) \text{e}^2\text{fm}^4$  have been obtained for  $^{46}\text{Ar}$  from an absolute measurement, and from a measurement relative to that of  $^{44}\text{Ca}$ , respectively. These two values are, within about one  $\sigma$ , in accordance with the  $B(E2)$  of  $196(39) \text{e}^2\text{fm}^4$  and  $218(31) \text{e}^2\text{fm}^4$  obtained in Refs. [2] and [20], respectively. Combining these four measurements, a  $B(E2)$  value of  $216(22) \text{e}^2\text{fm}^4$  is proposed for  $^{46}\text{Ar}$ . This value is smaller, though still almost compatible within  $2\sigma$ , with the one obtained with marginal statistics by means of lifetime measurement ( $570_{-160}^{+335} \text{e}^2\text{fm}^4$ ). This value of  $216(22) \text{e}^2\text{fm}^4$  is about a factor of two smaller than the results of shell model calculations, whatever the choice of interaction. This deviation between experiment and shell model calculations for  $^{46}\text{Ar}$  at  $N = 28$ , that is only two protons below  $^{48}\text{Ca}$ , is even more surprising since all  $E(2_1^+)$  energies in the Ar isotopes from  $N = 20$  to the newly studied  $N = 30$   $^{48}\text{Ar}$  [53,55] are rather well reproduced by the same calculations. Analyzing the contributions of the proton and neutron  $A_{p,n}^2$  transition matrix elements, it is proposed that the major reason for the discrepancy between experimental and

calculated  $B(E2)$  at  $N = 28$  resides in the over-prediction of the proton contribution  $A_p^2$ .

#### ACKNOWLEDGMENTS

The authors are grateful for the financial support from the European Social Fund through POSDRU Project No.

107/1.5/S/82514. This work was supported by the Romanian National Authority grant for Scientific Research, CNCS - UEFISCDI, Project No. PN-II-RU-TE-2011-3-0051, the Hungarian Scientific Research Fund OTKA (Grant No. K100835) and STFC (U.K.). We are grateful for the technical support provided by the GANIL facility staff.

- 
- [1] O. Sorlin and M.-G. Porquet, *Phys. Scr. T* **152**, 014003 (2013).
- [2] H. Scheit, T. Glasmacher, B. A. Brown, J. A. Brown, P. D. Cottle, P. G. Hansen, R. Harkewicz, M. Hellstrom, R. W. Ibbotson, J. K. Jewell, K. W. Kemper, D. J. Morrissey, M. Steiner, P. Thiroff, and M. Thoennessen, *Phys. Rev. Lett.* **77**, 3967 (1996).
- [3] T. Glasmacher *et al.*, *Phys. Lett. B* **395**, 163 (1997).
- [4] B. Bastin, S. Grevy, D. Sohler, O. Sorlin, Z. Dombradi, N. L. Achouri, J. C. Angelique, F. Azaiez, D. Baiborodin, R. Borcea, C. Bourgeois, A. Buta, A. Burger, R. Chapman, J. C. Dalouzy, Z. Dlouhy, A. Drouard, Z. Elekes, S. Franchoo, S. Jacob, B. Laurent, M. Lazar, X. Liang, E. Lienard, J. Mrazek, L. Nalpas, F. Negoita, N. A. Orr, Y. Penionzhkevich, Z. Podolyak, F. Pougheon, P. Roussel-Chomaz, M. G. Saint-Laurent, M. Stanoiu, I. Stefan, F. Nowacki, and A. Poves, *Phys. Rev. Lett.* **99**, 022503 (2007).
- [5] S. Takeuchi, M. Matsushita, N. Aoi, P. Doornenbal, K. Li, T. Motobayashi, H. Scheit, D. Steppenbeck, H. Wang, H. Baba, D. Bazin, L. Caceres, H. Crawford, P. Fallon, R. Gernhauser, J. Gibelin, S. Go, S. Grevy, C. Hinke, C. R. Hoffman, R. Hughes, E. Ideguchi, D. Jenkins, N. Kobayashi, Y. Kondo, R. Krucken, T. LeBlais, J. Lee, G. Lee, A. Matta, S. Michimasa, T. Nakamura, S. Ota, M. Petri, T. Sako, H. Sakurai, S. Shimoura, K. Steiger, K. Takahashi, M. Takechi, Y. Togano, R. Winkler, and K. Yoneda, *Phys. Rev. Lett.* **109**, 182501 (2012).
- [6] S. Péru *et al.*, *Eur. Phys. J. A* **9**, 35 (2000).
- [7] R. Rodríguez-Guzmán, J. L. Egido and L. M. Robledo, *Phys. Rev. C* **65**, 024304 (2002).
- [8] Z. P. Li, J. M. Yao, D. Vretenar, T. Niksic, H. Chen, and J. Meng, *Phys. Rev. C* **84**, 054304 (2011).
- [9] S. Ebata and M. Kimura, *Phys. Rev. C* **91**, 014309 (2015).
- [10] F. Nowacki and A. Poves, *Phys. Rev. C* **79**, 014310 (2009).
- [11] L. Gaudefroy, *Phys. Rev. C* **81**, 064329 (2010).
- [12] K. Kaneko, Y. Sun, T. Mizusaki, and M. Hasegawa, *Phys. Rev. C* **83**, 014320 (2011).
- [13] Y. Utsuno, T. Otsuka, B. A. Brown, M. Honma, T. Mizusaki, and N. Shimizu, *Phys. Rev. C* **86**, 051301 (2012).
- [14] R. Chevrier and L. Gaudefroy, *Phys. Rev. C* **89**, 051301 (2014).
- [15] C. Force, S. Grevy, L. Gaudefroy, O. Sorlin, L. Caceres, F. Rotaru, J. Mrazek, N. L. Achouri, J. C. Angelique, F. Azaiez, B. Bastin, R. Borcea, A. Buta, J. M. Daugas, Z. Dlouhy, Z. Dombradi, F. DeOliveira, F. Negoita, Y. Penionzhkevich, M. G. Saint-Laurent, D. Sohler, M. Stanoiu, I. Stefan, C. Stodel, and F. Nowacki, *Phys. Rev. Lett.* **105**, 102501 (2010).
- [16] Z. Meisel, S. George, S. Ahn, J. Browne, D. Bazin, B. A. Brown, J. F. Carpino, H. Chung, R. H. Cyburt, A. Estrade, M. Famiano, A. Gade, C. Langer, M. Matos, W. Mittig, F. Montes, D. J. Morrissey, J. Pereira, H. Schatz, J. Schatz, M. Scott, D. Shapira, K. Smith, J. Stevens, W. Tan, O. Tarasov, S. Towers, K. Wimmer, J. R. Winkelbauer, J. Yurkon, and R. G. T. Zegers, *Phys. Rev. Lett.* **114**, 022501 (2015).
- [17] L. Gaudefroy, J. M. Daugas, M. Hass, S. Grevy, C. Stodel, J. C. Thomas, L. Perrot, M. Girod, B. Rosse, J. C. Angelique, D. L. Balabanski, E. Fiori, C. Force, G. Georgiev, D. Kameda, V. Kumar, R. L. Lozeva, I. Matea, V. Meot, P. Morel, B. S. Nara Singh, F. Nowacki, and G. Simpson, *Phys. Rev. Lett.* **102**, 092501 (2009).
- [18] J. Lee, M. B. Tsang, D. Bazin, D. Coupland, V. Henzl, D. Henzlova, M. Kilburn, W. G. Lynch, A. M. Rogers, A. Sanetullaev, A. Signoracci, Z. Y. Sun, M. Youngs, K. Y. Chae, R. J. Charity, H. K. Cheung, M. Famiano, S. Hudan, P. O'Malley, W. A. Peters, K. Schmitt, D. Shapira, and L. G. Sobotka, *Phys. Rev. Lett.* **104**, 112701 (2010).
- [19] A. Gade, D. Bazin, C. A. Bertulani, B. A. Brown, C. M. Campbell, J. A. Church, D. C. Dinca, J. Enders, T. Glasmacher, P. G. Hansen, Z. Hu, K. W. Kemper, W. F. Mueller, H. Olliver, B. C. Perry, L. A. Riley, B. T. Roeder, B. M. Sherrill, J. R. Terry, J. A. Tostevin, and K. L. Yurkewicz, *Phys. Rev. C* **71**, 051301 (2005).
- [20] A. Gade, D. Bazin, C. M. Campbell, J. A. Church, D. C. Dinca, J. Enders, T. Glasmacher, Z. Hu, K. W. Kemper, W. F. Mueller, H. Olliver, B. C. Perry, L. A. Riley, B. T. Roeder, B. M. Sherrill, and J. R. Terry, *Phys. Rev. C* **68**, 014302 (2003).
- [21] A. Gade, B. A. Brown, D. Bazin, C. M. Campbell, J. A. Church, D. C. Dinca, J. Enders, T. Glasmacher, M. Horoi, Z. Hu, K. W. Kemper, W. F. Mueller, T. Otsuka, L. A. Riley, B. T. Roeder, T. Suzuki, J. R. Terry, K. L. Yurkewicz, and H. Zwahlen, *Phys. Rev. C* **74**, 034322 (2006).
- [22] D. Mengoni, J. J. Valiente-Dobon, A. Gadea, S. Lunardi, S. M. Lenzi, R. Broda, A. Dewald, T. Pissulla, L. J. Angus, S. Aydin, D. Bazzacco, G. Benzoni, P. G. Bizzeti, A. M. Bizzeti-Sona, P. Boutachkov, L. Corradi, F. Crespi, G. deAngelis, E. Farnea, E. Fioretto, A. Goergen, M. Gorska, A. Gottardo, E. Gardner, A. M. Howard, W. Krolas, S. Leoni, P. Mason, D. Montanari, G. Montagnoli, D. R. Napoli, A. Obertelli, R. Orlandi, T. Pawlat, G. Pollarolo, F. Recchia, A. Algora, B. Rubio, E. Sahin, F. Scarlassara, R. Silvestri, J. F. Smith, A. M. Stefanini, D. Steppenbeck, S. Szilner, C. A. Ur, P. T. Wady, and J. Wrzesinski, *Phys. Rev. C* **82**, 024308 (2010).
- [23] J. Retamosa, E. Caurier, F. Nowacki, and A. Poves, *Phys. Rev. C* **55**, 1266 (1997).
- [24] S. Nummela, P. Baumann, E. Caurier, P. Dessagne, A. Jokinen, A. Knipper, G. LeScornet, C. Miehe, F. Nowacki, M. Oinonen, Z. Radivojevic, M. Ramdhane, G. Walter, and J. Aysto, *Phys. Rev. C* **63**, 044316 (2001).
- [25] R. Anne *et al.*, *Nucl. Instrum. Methods A* **257**, 215 (1987).
- [26] S. Ottini *et al.*, *Nucl. Instrum. Methods A* **431**, 476 (1999).
- [27] A. N. Ostrowski *et al.*, *Nucl. Instrum. Methods A* **480**, 448 (2002).
- [28] S. Agostinelli *et al.*, *Nucl. Instr. Meth. Phys. Res. A* **506**, 250 (2003).
- [29] S. Leenhardt *et al.*, *Eur. Phys. J. A* **14**, 1 (2002).

- [30] C. Bertulani, C. M. Campbell, and T. Glasmacher, *Comput. Phys. Commun.* **152**, 317 (2003).
- [31] W. W. Wilcke *et al.*, *At. Data Nucl. Data Tables* **25**, 389 (1980).
- [32] F. W. N. de Boer *et al.*, *Z. Phys. A Atom. Nucl.* **325**, 457 (1986).
- [33] A. Winther and K. Alder, *Nucl. Phys. A* **319**, 518 (1979).
- [34] J. D. Jackson, *Classical Electrodynamics* (Wiley, New York, 1974), p. 620.
- [35] T. Suomijärvi *et al.*, *Nucl. Phys. A* **509**, 369 (1990).
- [36] S. Raman, C. W. Nestor, and P. Tikkanen, *Atom. Data Nucl. Data Tables* **78**, 1 (2001).
- [37] M. Bini *et al.*, *Lett. Nuov. Cim.* **5**, 913 (1972).
- [38] C. W. Towsley, D. Cline and R. N. Horoshko, *Nucl. Phys. A* **204**, 574 (1973).
- [39] H. Gruppelaar and P. J. M. Smulders, *Nucl. Phys. A* **179**, 737 (1972).
- [40] T. R. Fischer and P. D. Bond, *Part. Nucl.* **6**, 119 (1973).
- [41] J. D. McCullen and D. J. Donahue, *Phys. Rev. C* **8**, 1406 (1973).
- [42] J. Heisenberg *et al.*, *Nucl. Phys. A* **164**, 353 (1971).
- [43] K. Itoh *et al.*, *Nucl. Phys. A* **492**, 426 (1989).
- [44] M. J. A. de Voigt *et al.*, *Phys. Rev. C* **10**, 1798 (1974).
- [45] J. Chen, B. Singh, and J. A. Cameron, *Nucl. Data Sheets* **112**, 2357 (2011).
- [46] A. M. Bernstein, in *Adv. in Nucl. Phys.*, edited by M. Baranger and E. Vogt, Vol. 3 (Plenum Press, New York, 1969), p. 325.
- [47] Z. Dombrádi *et al.*, *Nucl. Phys. A* **727**, 195 (2003).
- [48] L. Gaudefroy, O. Sorlin, F. Nowacki, D. Beaumel, Y. Blumenfeld, Z. Dombrádi, S. Fortier, S. Franchoo, S. Grevy, F. Hammache, K. W. Kemper, K. L. Kratz, M. G. S. Laurent, S. M. Lukyanov, L. Nalpas, A. N. Ostrowski, Y. E. Penionzhkevich, E. C. Pollacco, P. Roussel, P. Roussel-Chomaz, D. Sohler, M. Stanoiu, and E. Tryggestad, *Phys. Rev. C* **78**, 034307 (2008).
- [49] NuShellX@MSU, B. A. Brown, W. D. M. Rae, E. McDonald, and M. Horoi, <http://www.nucl.msu.edu/~brown/resources/resources.html>.
- [50] E. Khan *et al.*, *Nucl. Phys. A* **694**, 103 (2001).
- [51] L. A. Riley, M. A. Abdelqader, D. Bazin, M. J. Bojazi, B. A. Brown, C. M. Campbell, J. A. Church, P. D. Cottle, D. C. Dinca, J. Enders, A. Gade, T. Glasmacher, M. Honma, S. Horibe, Z. Hu, K. W. Kemper, W. F. Mueller, H. Olliver, T. Otsuka, B. C. Perry, B. T. Roeder, B. M. Sherrill, T. P. Spencer, and J. R. Terry, *Phys. Rev. C* **72**, 024311 (2005).
- [52] A. M. Bernstein, V. R. Brown, and V. A. Madsen, *Phys. Rev. Lett.* **42**, 425 (1979).
- [53] R. Winkler, A. Gade, T. Baugher, D. Bazin, B. A. Brown, T. Glasmacher, G. F. Grinyer, R. Meharchand, S. McDaniel, A. Ratkiewicz, and D. Weisshaar, *Phys. Rev. Lett.* **108**, 182501 (2012).
- [54] B. A. Brown and B. H. Wildenthal, *Phys. Rev. C* **21**, 2107 (1980).
- [55] S. Bhattacharyya, M. Rejmund, A. Navin, E. Caurier, F. Nowacki, A. Poves, R. Chapman, D. O'Donnell, M. Gelin, A. Hodsdon, X. Liang, W. Mittig, G. Mukherjee, F. Rejmund, M. Rousseau, P. Roussel-Chomaz, K. M. Spohr, and C. Theisen, *Phys. Rev. Lett.* **101**, 032501 (2008).